Flory-Huggins Photonic Sensors

Paola Lova,[1*] Giovanni Manfredi,[1○] Chiara Bastianini, [1] Carlo Mennucci,[2] Francesco Buatier de Mongeot, [2] Alberto Servida[1] and Davide Comoretto[1#]

[1] Dipartimento di Chimica e Chimica Industriale and [2] Dipartimento di Fisica, Università degli Studi di Genova, Via Dodecaneso 31, 16146, Genova, Italy.

○Present Address: Center for Nano Science and Technology, Istituto Italiano di Tecnologia, Via Giovanni Pascoli 70, 20133 Milano, Italy

#E-mail: davide.comoretto@unige.it

*E-mail paola.lova@edu.unige.it

The lack of cost-effective systems for the extensive assessment of air pollutants is a concern for health and safety in urban and industrial areas. The use of polymer thin films as label-free colorimetric sensors featuring specific interactions with pollutants would then represent a paradigm shift in environmental monitoring and packaging technologies, allowing to assess air quality, formation of byproducts in closed environment, and the barrier properties of the polymer themselves. To this end, all-polymer distributed Bragg reflectors promises reliable transducers for chemical stimuli, and effective colorimetric label-free selective detectors. We show selectivity attained by specific interaction of the polymeric components with the analytes. Such interactions drive the analyte intercalation trough the polymer structure and its kinetics, converting it in a dynamic optical response which is at the basis of the Flory-Huggins photonic sensors. Additionally, we demonstrate that such optical response can be used to esteem the diffusion coefficients of small molecules within the polymer media via simple UV-Vis spectroscopy retrieving data comparable to those obtained with state of the art gravimetric procedures. These results pave the way to an innovative, simple, and low-cost detection method integrable to *in-situ* assessment of barrier polymers used for the encapsulation of optoelectronic devices, food packaging, and goods storage in general.

Currently, barrier properties of polymer thin films to vapors and gas are assessed via gravimetric[1] and pressure decay methods,[2-4] or by optical techniques based on microscopy[5] and infrared absorption,[6] which remained substantially unchanged for the last few decades. These methods need dedicated equipment and cannot be performed *in-situ.* In this scenario, research for new low-cost, simpler, and portable technologies to gather lab-on-chip devices is strongly pursued. In these regards, sensors based on the optical response of polymer distributed Bragg reflectors (DBR) represent a possible revolution in the field due to the high responsivity to analytes in the vapor phase.[7-9] DBRs are planar photonic crystals made of media with different refractive index stacked to form a dielectric lattice. The interaction between light and DBRs induces frequency regions where light propagation is forbidden. These frequencies are called photonic band gaps (PBGs), and are easily detectable via simple reflectance or transmittance spectroscopy.[10] In analogy with the energy-gap of semiconductors, the PBG properties depend on the lattice structure. Then, dielectric contrast among the lattice components, lattice parameters, and the number of layers affect the optical features generated by the DBR photonic structure.[11] Intuitively, a perturbation of

these parameters, affects the entire photonic crystal spectrum, and then its variation can be related to the stimuli such as pressure variations,[12,13] chemical analytes,[8,9,14-17] and pH.[18]

Unlike meso-porous DBR sensors,[10,17,19,20] polymer structures often play as dense membrane and molecular diffusion is ruled by the analyte solubility in the polymer matrices.[8] Therefore, to diffuse within the structure and affect the DBR optical response, the analyte needs to be solubilized within the dense polymer and then diffuse through it. The molecular species must then have chemico-physical affinity with the dense matrix. Such affinity can be defined by the Flory-Huggins parameter for the analyte-polymer pairs (χ_{AP}^{H}, neglecting entropic contribution), which can be expressed as a function of analyte molar volume (V^M) and the solubility parameter for the pair.[21-24] The latter is defined from the Hildebrand parameters of the two components of the mixtures (δ_P, δ_A) as $\Delta\delta^2 = (\delta_P - \delta_A)^2$, and expresses the difference of cohesive energy between the analytes and the polymers, the smaller is $\Delta\delta^2$, the larger is the solubility.[21,22]

$$\chi_{AP}^{H} = V^M \frac{\Delta\delta^2}{RT} \quad (1)$$

where R is the gas constant and T the temperature. For this reason, all-polymer DBR can be called Flory-Huggins photonic sensors (FHPS).[19] Then, the choice of suitable polymers as active media makes them efficient detectors for the label-free identification of a variety of analytes in the vapor phase, and allows to extend the method to a large amount of chemical species, including water, toxic and carcinogenic volatile organic compounds and even perfluorinated species,[7,9,25-30] paving the way for a new generation of photonic sensors with novel capabilities and broad band selectivity.

In this work, we propose an original proof of concept FHPS device made of commodity polymers for the evaluation of the diffusion coefficients of molecular species into polymer matrices and their discrimination to assess air quality. We demonstrate for the first time that DBRs-based FHPS made of polystyrene (PS) and cellulose acetate (CA) discriminate between air enriched with different short chain alcohols, including methanol (MeOH), Ethanol (EtOH), *1*-propanol (1POH), *2*-propanol (2POH), and *1*-buthanol (1BuOH). These analytes were chosen for two reasons. First,

their discrimination is extremely challenging since the molecules have similar molecular weight and present comparable Van der Waals volumes, polarity, hydrogen bonding, and volatility. Second, the ability to disentangle these alcohols and to study polymer barrier properties is of extraordinary importance to prevent toxic effects. Indeed, while EtOH is widely used in food industry, MeOH, which is a byproduct of EtOH fermentation, generates toxic effects in both the acute and the cronic forms[31] due to its metabolization to formaldehyde and formic acid.[32,33] Moreover, 1POH and 2POH share a similar structure, physical properties, and applications, but 2POH is less toxic than 1POH and finds applications in many antibacterial and personal care products.[33] Similarly, 1BuOH, which is interesting for biofulel,[34] shows a very low toxicity, but causes eye and skin irritation and is harmful if inhaled.[33]

Working principle of FHPSs

The FHPSs under investigation are made of 31 alternated layers of PS and CA, as sketched in Figure 1a. Such structures provide a typical optical response, shown as a black line in the reflectance spectrum of Figure 1b. The spectrum displays two maxima of reflectance at 845 nm and 430 nm. These features are assigned to the FHPS PBG and to its second order replica. When the FHPS is placed in air polluted with a volatile molecular compound, the molecules permeate into its structure, and progressively swell the PS, the CA or both the layers, depending on χ_{ap}^{H}.[7-9] The interaction between the polymer and the analyte results in a variation of the thickness and refractive index of the layers, and thus, of the light optical path (Figure 1a). In turn, such variation affects the PBG spectral position, according to

$$\lambda_{PBG} = 2\sqrt{d_L + d_H}\sqrt{d_L n_L^2 + d_H n_H^2} \quad (2)$$

where d and n are the thickness and the refractive index of the low (d_L, n_L) and high refractive index layers $(d_H n_H)$. Indeed, the red line spectrum of Figure 1b shows that after 90 min of exposure to MeOH (see Methods for details) the first order PBG of the FHPS red-shifts of about 100 nm to 940 nm, while the second order PBG shifts of about 50 nm to 475 nm.[35]

Figure 1c illustrates the dynamics of the optical response as a contour plot where the exposure time and the wavelength are represented as the y- and as the x- axis respectively, while the reflectance intensity is reported as a color code. As mentioned above, the first and second order PBGs are initially located at 845 nm and 430 nm, respectively. These features are visible in red-tones, while the spectra background is represented in blue tones. The red-shift of the PBGs is initially very fast, and reaches ~80% of the final value within the first 10 min of exposure. Then, the dynamics slows down, and the system reaches the equilibrium in 90 min. To highlight the temporal evolution of PBG spectral positions, in Figure 1d we show the maximum of intensities of each spectrum, which correspond to the two spectral features, versus the exposure time. These data represent then the dynamic evolution of the first (blue line) and second (green line) order PBGs after normalization by the respective value of shift observed at the steady-state (~90 min, $\Delta\lambda_{1\infty}$ = 100 nm and $\Delta\lambda_{2\infty}$ =50 nm for the first and second order PBG respectively).

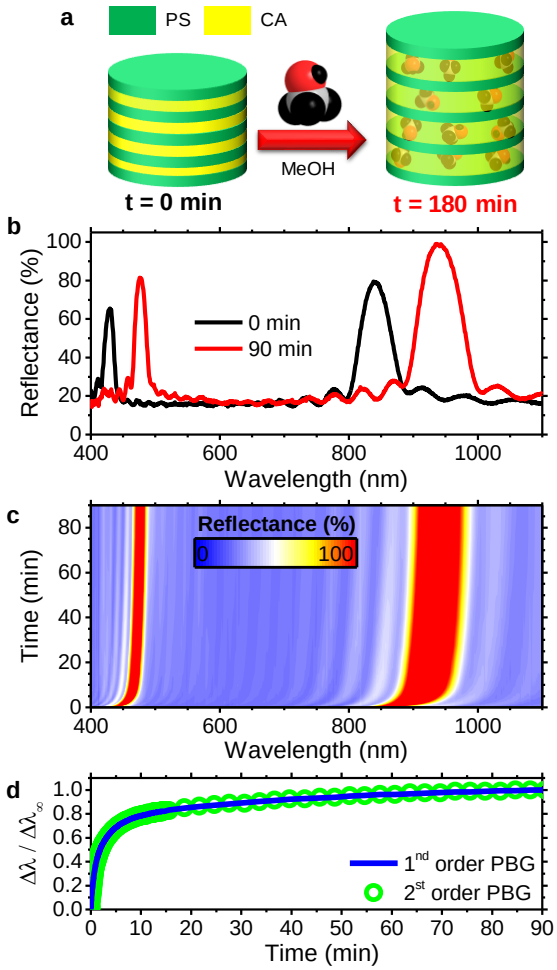

Figure 1: Scheme of the intercalation of MeOH into a PS:CA FHPS where only CA swells, b) reflectance spectra of a DBR before (black line) and after (red line) 90 min of exposure in MeOH environment, c) contour-plot of the temporal evolution of the FHPS spectra during the MeOH exposure, and d) normalized profile of the first (blue line) and second (open dots) order PBGs spectral position during the exposure.

The dynamic responses of Figure 1d are similar to the gravimetric sorption curves retrieved from diffusive processes in polymer slabs.[36] Indeed, the penetration of a molecular species into the polymer films and their possible swelling affect both the refractive indexes (n_{PS} and n_{CA}) and the geometrical thicknesses (d_{PS} and d_{CA}) of the layers composing the FHPS. In turn, their optical thickness ($n * d$) is modified. Because for vapor analytes $\Delta d/d(0) \gg \Delta n/n(0)$,[8,37] we can

assume that the refractive index variation is negligible during the swelling process, $n(0) \approx n(t) \approx n(\infty)$. Then, we can derive that the absorbed vapor mass, M(t), is proportional to the variation of thickness, which in turn affects the PBG spectral position.

$$\frac{M(t)}{M(\infty)} \div \frac{d(t)-d(0)}{d(\infty)-d(0)} \div \frac{\Delta\lambda_1(t)}{\Delta\lambda_1(\infty)}, \frac{\Delta\lambda_2(t)}{\Delta\lambda_1(\infty)} \quad (3)$$

where $M(\infty)$ is the mass of the molecular species permeated through the polymer film at the equilibrium obtained for an infinite exposure time ($t \to \infty$), $d = d_{PS} + d_{CA}$, $\Delta\lambda_1$and $\Delta\lambda_2$ are respectively the spectral shift of the first and second order PBGs at time t and at the equilibrium.

The sorption rate of a molecular species through a medium typically exhibits two regimes: a non-steady-state one, which is regulated by the diffusivity of the molecules within the polymer matrix, and a steady-state one, which depends upon their equilibrium solubility at saturation. Standard gravimetric methods consist in the exposure of a supported polymer film at constant temperature, volume, and at a defined initial vapor pressure. In such measurements, the dynamics of the pressure variation is correlated to the polymer mass intake, which determines the equilibrium solubility at the steady state and by the diffusivity at the non-steady state. For a thin polymer slab with thickness *d*, such that the diffusion of the molecular species cannot occour through the sides (one-dimensional diffusion), the variation of concentration c(z,t) along the *z* axis can be described by the second Fick's law, $\frac{\partial c}{\partial t} = \left(\mathcal{D}\frac{\partial^2 c}{\partial z^2}\right)$, where $\mathcal{D}$ is the diffusion coefficient, c is the concentration of the molecular species within the slab and z is the diffusion distance. The boundary conditions are c(z,t) = 0 at t=0 for each z, then at $t > 0$ the surface concentration is equal to the equilibrium one, and $\frac{\partial c}{\partial z} = 0$ at $z = d$ for each t. Following this approach, one can espress the mass intake as decribed by Crank:[36,38]

$$\frac{M(t)}{M(\infty)} = \frac{\Delta\lambda(t)}{\Delta\lambda(\infty)} = \sqrt{\frac{Dt}{d^2}}\left(\sqrt{\pi} + 2\sum_{n=1}^{\infty}(-1)^n ierf\left(\frac{nd}{2\sqrt{Dt}}\right)\right) \quad (4)$$

where $ierf$ is the complex error function.[36] For short exposure time, where $M(t)/M(\infty) < 0.2$ the second term of Equation 4 can be neglected, and:[6,39]

$$\frac{\Delta\lambda(t)}{\Delta\lambda(\infty)} = \frac{2}{d}\sqrt{\frac{\mathcal{D}}{\pi}}\sqrt{t}. \quad (5)$$

Therefore, $\mathcal{D}$ can be evaluated from the angular coefficient of the linear part of the sorption curve of Figure 1d, reported as $\Delta\lambda(t)/\Delta\lambda(\infty)$ vs. $\sqrt{t}$. This approach assumes constant thickness of the polymer slab. Within the time domain considered to determine $\mathcal{D}$, the thickness variation is below 20% of the total value, which makes the assumption reasonable.

Optical Assesment of D_{eff}

In a previous work, we demonstrated that the kinetics of the intercalation process just described strongly depends on the interactions that occour between the polymers and the analyte.[9] Indeed, parameters like the analyte Van der Waals volume, polarity, and the fomation of hydrogen bonds affect the analyte permeation rate in the polymer layers, their swelling degree, and in turn the optical response of the FHPS. Then, the possibility to relate the permeation kinetics of the molecular species to the simple FHPS optical response paves the way develop a new powerful tool for the simple determination of vapor diffusivity into polymer multilayers, also suitable for *in-situ* measurements without chemical functionalizations. Indeed, these systems are also efficient label-free selective sensors for vapor analytes, that could make colorimetric sensors suitable for safety devices in the food industry, industrial air pollution, households, and offices.[9]

As a proof-of-concept, beside MeOH, we investigated a chemical series of short chain alcohols with chemico-physical properties scaling with the number of carbons. To evaluate the optical response of the sensors, a FHPS made of 31 layers of PS and CA was divided into five portions, which were exposed to the alcohols mentioned above in a closed environment at room condition to simulate real operating conditions. The evolution of the FHPS spectrum was sampled at a given

frequency (see Methods section). The collected spectra are reported, described and analysed in Supplementary Figure S1. These spectra and the retrieved optical dynamic responses show that the rate of the permeation process is characteristic and alcohol-dependent, thus allowing their label-free recognition.

Figure 2 shows the optical sorption curves retrieved from the contour plots for the response to the five alcohols reported in Supplementary Figure S1. The curves show two main behaviors; the first one, which characterizes the sorption of MeOH and EtOH, consists in a linear increase of the analyte intake followed by the steady-state regime. The second, observed for 1POH, 2POH and 1BuOH, is characterized by the presence of discontinuities in the PBG position that occurs both at the steady and at the non-steady state regimes, in agreement with previous findings: while in the case of MeOH and EtOH the swelling of all the FHPS layers occur almost simultaneously, in the case of alcohols with larger steric hindrance, the intercalation is slower, and the polymers are gradually swollen from the top layer of the FHPS in contact with air to the bottom one in contact with the substrates.[8,9] The presence of swollen and un-swollen layers breaks the DBR order destroying the condition that generates the PBG and its optical response and creating those discontinuities.

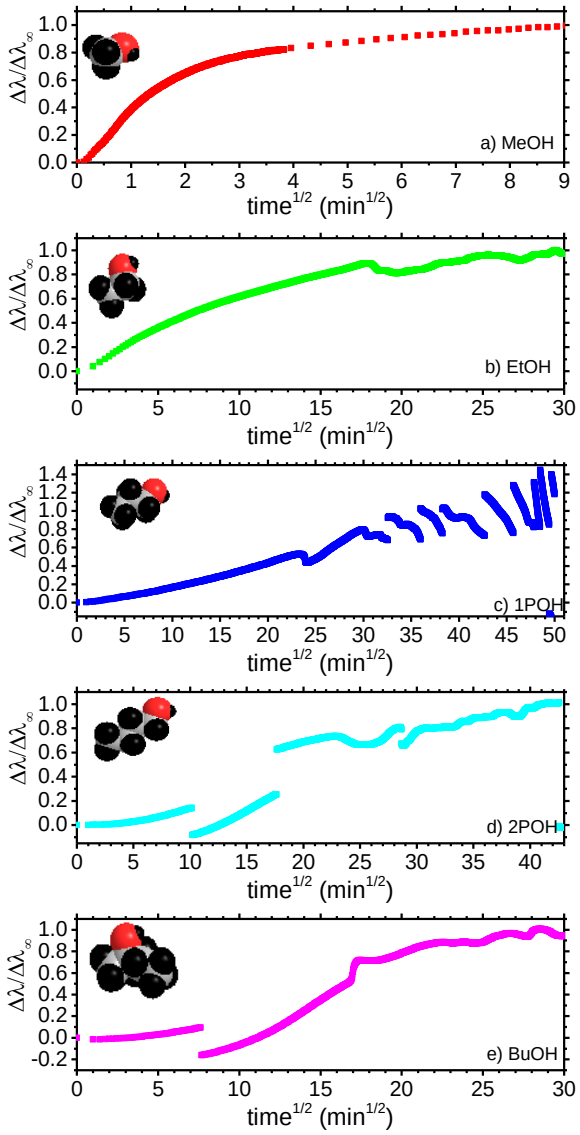

Figure 2: Normalized spectral profile of the spectral position for the FHPS first order PBG versus the square root of the exposure time to: a) MeOH, b) EtOH, c) 1POH, d) 2POH, and e) 1BuOH.

The optical sorption curves can be used to assess the effective diffusion coefficient of the analytes in the whole polymer composite ($\mathcal{D}_{eff}$). According to Equations 5, one needs to evaluate the angular coefficient of the sorption curves of Figure 2, and the initial thickness of the FHPS at t = 0. The latter was estimated modelling the FHPS reflectance spectrum[9,26,40] as described in Supplementary Figure 3, the total FHPS thickness can be estimated as 4.3 x 10^{-4} cm. The slope of the optical sorption curves has then been retrieved within their interval of linearity (Figure 2),

while the value of $\Delta\lambda_\infty$ was evaluated as the average $\Delta\lambda$ in the plateau region of the curves reported in Supplementary Figure 1 a"-c".

Table 1: Steric and chemico-physical parameters of the species and retrieved $\mathcal{D}_{eff}$.

	v (Å^3)[22]	δ (MPa$^{1/2}$) [21,41-43]	χ^H_{eff}	$\Delta\lambda_\infty$ (nm)	$\mathcal{D}_{eff}$ (cm^2 min^{-1})
MeOH	67.6	29.6	1.22	100	$2.5*10^{-8}$
EtOH	97.1	26.1	0.81	141	$7.9*10^{-10}$
1POH	124.9	24.4	0.64	180	$3.8*10^{-11}$
2POH	127.5	23.6	0.56	182	$2.2*10^{-11}$
1BuOH	151.9	23.3	0.65	220	$4.2*10^{-11}$
PS	-	18.7	-	-	-
CA	-	27.2	-	-	-

v = Van der Waals volume, δ = Hildebrand parameter, χ^H_{eff} = effective Flory-Huggins parameter, $\Delta\lambda_\infty$ = PBG shift at the equilibrium, $\mathcal{D}_{eff}$ = effective diffusivity within the DBR.

The calculated values of $\mathcal{D}_{eff}$ are summarized in Table 1 and Figure 3a, where the data are also compared with results available in literature for MeOH and EtOH.[44,45] The diffusivity of MeOH in CA has been reported as 8-9 x 10^{-8} cm^{2}s^{-1} while for PS it is 1.4 x 10^{-8} cm^{2}s^{-1} (at 55°C),[25,37] in good agreement with the effective values retrieved for our composite PS-CA DBR. For EtOH, the literature proposes 1-7 x 10^{-10} cm^{2}s^{-1}for CA and 9 x 10^{-10} cm^{2}s^{-1} (at 55°C) for PS,[44,45] again in agreement with our data (see Figure 3). Concerning the other alcohols, 1POH shows diffusion coefficient of 3.8 x 10^{-11} cm^{2}s^{-1}, for 2POH we retrieved $2.2*10^{-11}$ cm^{2}s^{-1}, while for BuOH $4.2*10^{-11}$ cm^{2}s^{-1}.

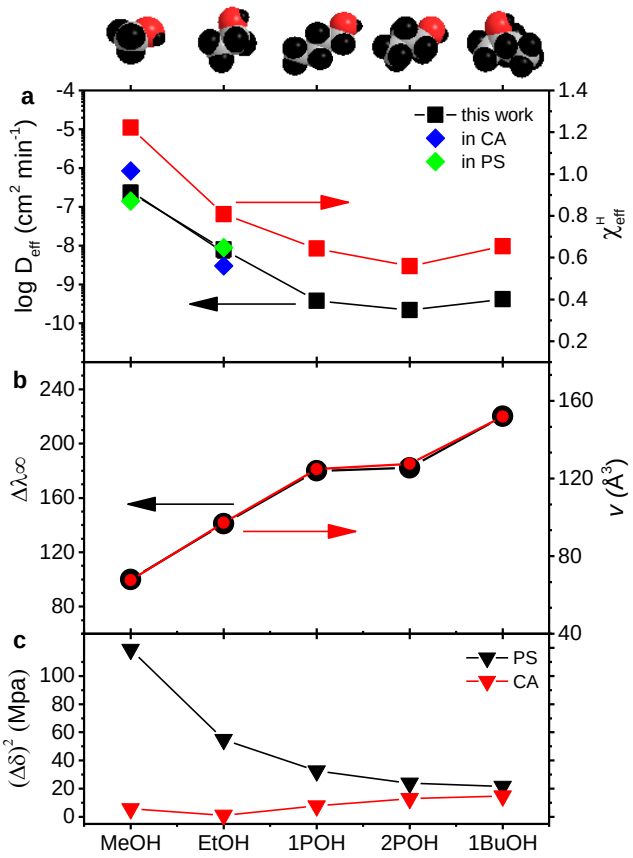

Figure 3: a, comparison between the retrieved value of $\mathcal{D}_{eff}$ (Equation 5) for the five alcohols (■) with literature data for CA (♦) and PS (♦),[44,45] and effective Flory-Huggins parameter (■, χ^{H}_{eff}). **b**, comparison of the FHPS $\Delta\lambda_{\infty}$ (●) for five alcohols and the alcohol Van der Waals volumes (●). **c**, Solubility parameters for the five alcohols with PS (▼) and CA (▼).

The behavior of the sorption curves, and in turn $\mathcal{D}_{eff}$, can be affected by the steric hindrance of the analyte molecules and by its chemico-physical affinity with the polymers. Figure 3a compares the values of $\mathcal{D}_{eff}$ with the effective FHPS-analytes Flory-Huggins parameters (χ^{H}_{eff}), calculated from Equation 1 considering the volume fraction of PS and CA within the DBR and neglecting the entropic contribution.[22] The panel b of the same Figure compares instead the FHPS PBG shift at the equilibrium, with Van Der Waals volume of the analytes. Interestingly, the Van der Waals volume values are strongly correlated to $\Delta\lambda_{\infty}$, and then to the polymer swelling (Equation 2). Conversely, there is a strong correlation between $\mathcal{D}_{eff}$ and χ^{H}_{eff}, and in turn with the solubility

parameters between the polymers and the analytes (Figure 3 a and c)[21] Figure 3c shows that the solubility of CA, within the alcohols is larger than for PS and it is roughly constant. Conversely, for PS $\Delta\delta^2$ decreases with the molecular weight of the alcohols, affecting also $\chi_{\mathrm{eff}}^{\mathrm{H}}$. These data prove that the decrease of $\mathcal{D}_{eff}$with the increase of the analyte molecular weight (panel a) is not linked by their solubility in the CA layers but in PS, which act as reservoir slowing down the analytes diffusion. Then, in the case of the most polar alcohols, CA plays as the sole active medium undergoing swelling, while the interaction between the analyte and PS can be considered negligible. This interpretation is also confirmed by the measurements of thickness variation upon MeOH exposure of single PS and CA films cast on glass substrates reported in Supporting Figure 2. When the films are exposed to MeOH vapors, CA swells dramatically, while PS thickness is not affected.

Label-Free Selectivity

This simple and powerful optical method for the determination of $\mathcal{D}_{eff}$ also applies to the discrimination of the analytes. Figure 2 and 3 show that even molecules with very similar structure and properties, such as 1POH and 2POH, provide a very different optical sorption kinetics and then different values of $\mathcal{D}_{eff}$. We would like to stress that the optical sorption curves, and more generally the dynamic of the overall FHPS optical responses are fingerprints characteristic of the analytes, that lead label-free discrimination and detection using simple DBR structures and low-cost optical setup.[8,9] Moreover, the large sensors spectral shifts make possible to discriminate the analytes also by the simple analysis of the spectral response at set times. This simple signal transduction allows colorimetric safety devices for air pollution suitable to detect the presence of an analyte in the vapor phase by un-trained users. As an example, Figure 4 shows the experimental spectra of the FHPS collected before and after 50 min of exposure to the five alcohols. While the sample initially shows two PBGs at ~845 nm and 430 nm, when exposed to MeOH, the PBGs width increases, and their spectral position shift to 931 nm and 474 nm, respectively. For EtOH the shift is smaller and the PBGs reaches 919 nm and 465 nm. 1POH instead provides a reduction of the peaks width which, after 10 min of exposures moves to 861 nm and 436 nm. Concerning 1BuOH, the alcohols with higher molecular weight, its intercalation induces disorder and inhomogeneous broadening of the PBGs, which reaches maxima of intensities at 860 nm and 425 nm after the exposure. The dynamics of these spectral responses are shown in Figure 4 b-d for the

five alcohols as contour plots. These patterns, which are described in detail in Supporting Figure S1, represents the characteristic polymer-solvent kinetic interaction, and can be unambiguously considered the fingerprint of the analyte detected with the specific FHPS.

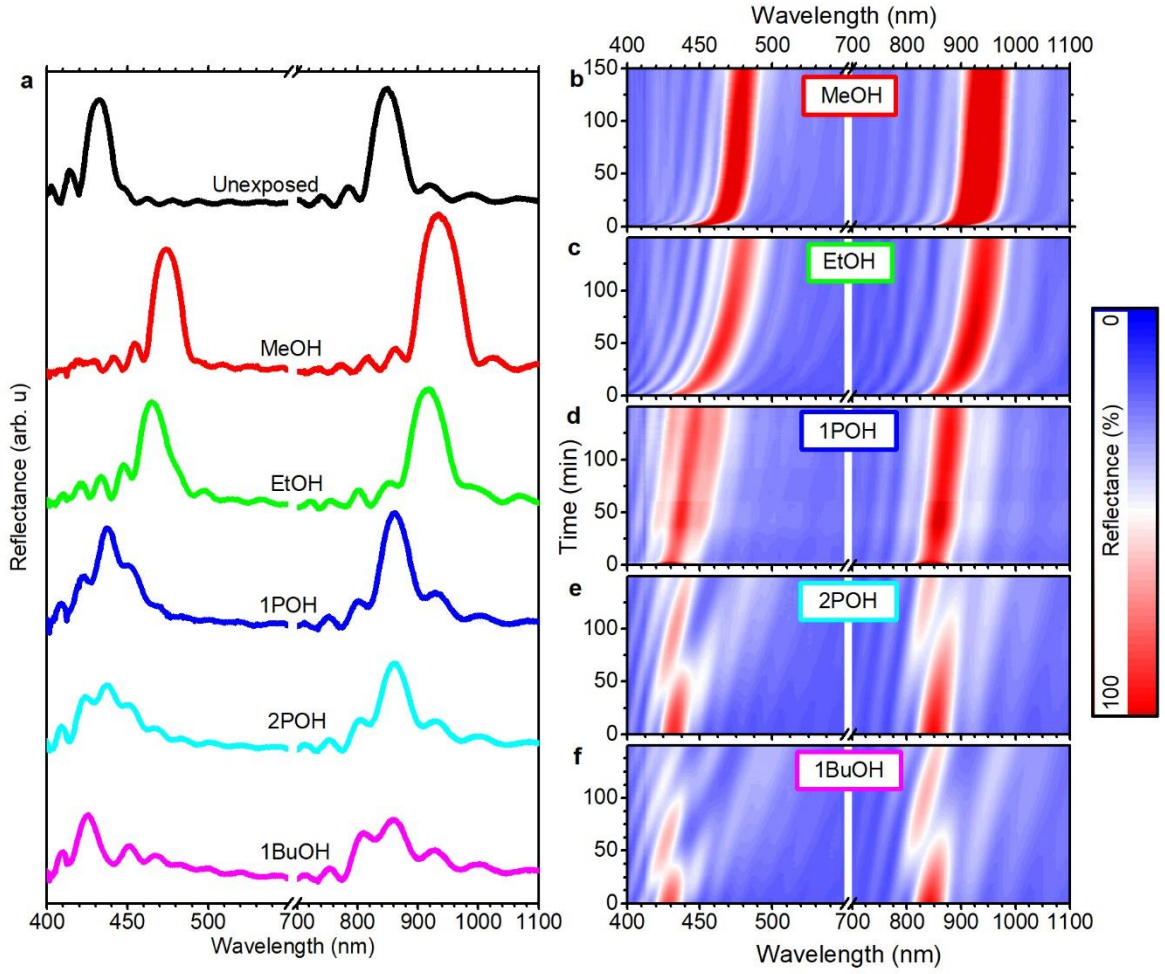

Figure 4: **a**, Reflectance spectra of the FHPS sensor before (black line) and after 50 min of exposure to MeOH (red line), EtOH (green line), 1POH (blue line), 2POH (cyan line), and 1BuOH (magenta line). Contour-plots of the dynamic FHPS response for: (**b**) MeOH, (**c**) EtOH, (**d**) 1POH, (**e**) 2POH, and (**f**) 1BuOH.

We would like to stress that the optical transductors here discussed are few millimeters in size and are fully processed from solution using commodity polymers, which can also be grown over square meters by coextrusion,[46-49] a technique widely used in the industrial production of packaging made of a large variety of polymers. Exploiting the fundamental thermodynamic of polymer-analyte mixtures allows then to engineer FHPSs affine with degradation by-products or harmful chemical

species. We envision their integration in smart packaging systems to monitor in-situ internal and external environments and assess diffusion of small molecules. This will also be possible thanks to small and compact detection systems already available to the market.[50,51]

CONCLUSIONS

This work provides an unprecedentedly powerful and versatile tool for the optical determination of the effective diffusion coefficients of vapor analytes within simple multilayered polymer distributed Bragg reflectors in excellent agreement with those reported in literature. The analysis of the kinetics can also be related to the chemico-physical interaction between the analyte and the polymers allowing simple and label-free molecular recognition by FHPS engineered *ad hoc*. The optical behavior of a DBR made by commodity polymers, which are easy to integrate in smart packaging devices, has been fully investigated during the exposure to five short chain alcohols. The study of the dynamic optical responses of the FHPS allows to retrieve sorption curves characteristic of the analytes that provides their diffusion coefficients and permits their discrimination. Since the FHPSs are sensitive to a large variety of molecular species, these proof of concept devices are promising for the development of sensors to be used on-site for the assessment of environmental pollution and for smart packaging.

METHODS

Sample Preparation*:* Polymer fhpss were fabricated by spin-coating deposition of 31 alternated layers of cellulose acetate (Sigma-Aldrich, M_n = 50 000) and polystyrene (Sigma-Aldrich, M_w = 192 000) dissolved in 4-hydroxy-4-methylpentan-2-one and toluene, respectively. The solution concentration was ~3% w/w and the rotation speed during the deposition was kept at ~8000 RPM.

Characterization: For all the FHPS, reflectance data were collected with a homemade setup based on optical fibers. Reflectance data were collected with a reflectance fiber probe, an Avantes AvaSpec-2048 spectrometer (200−1150 nm, resolution 1.4 nm), and a deuterium−halogen Micropak DH2000BAL light source. More details are reported in Ref. [8,9]

The optical response of the sensors during the exposure to methanol, ethanol, 1-propanol, 2-propanol, and 1-buthanol was measured at ~ 26 °C (see Table 1 for details) and 1 atm in a closed container where a 0.5 mL of the analyte were previously placed to saturate the environment. The concentrations of the analytes in the vapor phase are reported in Table 1. The optical response was

recorded at set time intervals with the optical setup previously mentioned using a reflectance immersion probe.

Spectra Modeling: The modelling of the FHPS spectrum (Supplementary Figure 3) was performed with a Matlab® homemade code based on the transfer matrix method as reported in previous works.[8,9] We used the refractive index dispersion from literature[40] as inputs and the layer thickness as fitting parameter.

Author Contributions

AS, DC and PL conceived the project and designed the experiments. CB worked on the sample fabrications. Optical characterizations were performed by CB, CM, and PL. Data were analyzed and modelled by AS, DC, GM, and PL. AS, DC and FBM coordinated the work. The manuscript was written through contributions of all authors.

Acknowledgments

PL thanks the European Union's Horizon 2020 research and innovation program under the Marie Sklodowska-Curie grant agreement No 643238 (SYNCHRONICS: SupramolecularlY eNgineered arCHitectures for optoelectRonics and photONICS). Support by the Italian Ministry of University, Research and Instruction through the "Progetti di Ricerca di Rilevante Interesse Nazionale 2010−2011" Program (Materiali Polimerici Nanostrutturati con strutture molecolari e cristalline mirate, per tecnologie avanzate e per l'ambiente, 2010XLLNM3) is also acknowledged.

Competing interests

The authors declare no competing interests.

Materials & Correspondence

DC: davide.comoretto@unige.it

PL: paola.lova@edu.unige.it

References

1 Berens, A. R. & Hopfenberg, H. B. Diffusion of organic vapors at low concentrations in glassy PVC, polystyrene, and PMMA. *J. Membr. Sci.* **10**, 283-303 (1982).

2 Vopička, O., De Angelis, M. G. & Sarti, G. C. Mixed gas sorption in glassy polymeric membranes: I. CO2/CH4 and n-C4/CH4 mixtures sorption in poly(1-trimethylsilyl-1-propyne) (PTMSP). *J. Membr. Sci.* **449**, 97-108 (2014).

3 Felder, R. M. & Huvard, G. S. in *Methods in Experimental Physics* Vol. 16 (Ed. R. A. Fava) 315-377 (Academic Press, New York, 1980).

4 Flaconneche, B., Martin, J. & Klopffer, M. Transport properties of gases in polymers: experimental methods. *Oil Gas Sci. Technol.* **56**, 245-259 (2001).

5 Mráček, A. The measurement of polymer swelling processes by an interferometric method and evaluation of diffusion coefficients. *Int. J. Mol. Sci.* **11**, 532-543 (2010).

6 Ferrari, M.-C., Catalano, J., Giacinti Baschetti, M., De Angelis, M. G. & Sarti, G. C. FTIR-ATR Study of Water Distribution in a Short-Side-Chain PFSI Membrane. *Macromolecules* **45**, 1901-1912 (2012).

7 Lova, P. *et al.* Hybrid ZnO:polystyrene nanocomposite for all-polymer photonic crystals. *Phys. Status Solidi C* **12**, 158-162 (2015).

8 Lova, P. *et al.* Polymer distributed Bragg reflectors for vapor sensing. *ACS Photonics* **2**, 537-543 (2015).

9 Lova, P. *et al.* Label-free vapor selectivity in poly(p-phenylene oxide) photonic crystal sensors. *ACS Appl. Mater. Interfaces* **8**, 31941–31950 (2016).

10 Comoretto, D. *Organic and hybrid photonic crystals*. (Springer,Place Published, 2015).

11 Graham-Rowe, D. Tunable structural colour. *Nat. Photon.* **3**, 551-553 (2009).

12 Jewart, C. M. *et al.* Ultrafast femtosecond-laser-induced fiber Bragg gratings in air-hole microstructured fibers for high-temperature pressure sensing. *Opt. Lett.* **35**, 1443-1445 (2010).

13 Fang, Y. *et al.* Reconfigurable photonic crystals enabled by pressure-responsive shape-memory polymers. *Nat. Comm.* **6**, 7416 (2015).

14 Lee, J.-H. *et al.* 25th anniversary article: Ordered polymer structures for the engineering of photons and phonons. *Adv. Mater.* **26**, 532 - 569 (2013).

15 Hidalgo, N., Calvo, M. E., Colodrero, S. & Miguez, H. Porous one-dimensional photonic crystal coatings for gas detection. *IEEE Sensors J.* **10**, 1206-1212 (2010).
16 Potyrailo, R. A. *et al.* Morpho butterfly wing scales demonstrate highly selective vapour response. *Nat. Photon.* **1**, 123 (2007).
17 MacLeod, J. & Rosei, F. Sustainable sensors from silk. *Nat. Mater.* **12**, 98 (2013).
18 Wang, Z. *et al.* Biochemical-to-optical signal transduction by pH sensitive organic-inorganic hybrid Bragg stacks with a full color display. *J. Mater. Chem. C* **1**, 977-983 (2013).
19 Lova, P., Manfredi, G. & Comoretto, D. Advances in functional solution processed planar one-dimensional photonic crystals. *Adv. Opt. Mater. (Accepted)*(2018).
20 Potyrailo, R. A. *et al.* Towards outperforming conventional sensor arrays with fabricated individual photonic vapour sensors inspired by Morpho butterflies. *Nat. Commun.* **6**, 7959-7912 (2015).
21 Cowie, J. M. G. *Polymers: Chemistry and Physics of Modern Materials.*, (Chapman&Hall,Place Published, 1991).
22 Hansen, C. M. *Hansen solubility parameters: a user's handbook*. 2nd edn, (CRC press,Place Published, 2002).
23 Flory, P. J. *Principles of polymer chemistry*. (Cornell University Press,Place Published, 1953).
24 Flory, P. J. Thermodynamics of high polymer solutions. *J. Chem. Phys.* **9**, 660-660 (1941).
25 Lova, P. & Soci, C. in *Organic and hybrid photonic crystals* Vol. 1 (Ed. Davide Comoretto) Ch. 187-212, 493 (Springer, Cham, 2015).
26 Manfredi, G., Mayrhofer, C., Kothleitner, G., Schennach, R. & Comoretto, D. Cellulose ternary photonic crystal created by solution processing. *Cellulose* **23**, 2853-2862 (2016).
27 Convertino, A., Capobianchi, A., Valentini, A. & Cirillo, E. N. M. High reflectivity bragg reflectors based on a gold nanoparticle/teflon-like composite material as a new approach to organic solvent detection. *Sens. Actuators, B* **100**, 212-215 (2004).
28 Convertino, A., Capobianchi, A., Valentini, A. & Cirillo, E. N. M. A new approach to organic solvent detection: High-reflectivity bragg reflectors based on a gold nanoparticle/teflon-like composite material. *Adv. Mater.* **15**, 1103 - 1105 (2003).
29 Mönch, W., Dehnert, J., Prucker, O., Rühe, J. & Zappe, H. Tunable Bragg filters based on polymer swelling. *Appl. Opt.* **45**, 4284-4290 (2006).

30 Giusto, P. *et al*. Colorimetric detection of perfluorinated compounds by all-polymer photonic transducers *ACS Omega* **3**, 7517-7522 (2018).
31 Martin-Amat, G., McMartin, K. E., Hayreh, S. S., Hayreh, M. S. & Tephly, T. R. Methanol poisoning: Ocular toxicity produced by formate. *Toxicol. Appl. Pharmacol.* **45**, 201-208 (1978).
32 McMartin, K. E., Ambre, J. J. & Tephly, T. R. Methanol poisoning in human subjects. *Am. J. Med.* **68**, 414-418 (1980).
33 Patocka, J. & Kuca, K. Toxic alcohols: Aliphatic saturated alcohols. *Mil. Med. Sci. Lett.* **81**, 142-163 (2012).
34 Ezeji, T. C., Qureshi, N. & Blaschek, H. P. Bioproduction of butanol from biomass: from genes to bioreactors. *Curr. Opin. Biotechnol.* **18**, 220-227 (2007).
35 Scotognella, F. *et al*. in *Organic and hybrid photonic crystals* Vol. 1 (Ed. Davide Comoretto) Ch. 77-101, 493 (Springer, Cham, 2015).
36 Crank, J. *The mathematics of diffusion*. 2nd edn, (Oxford university press,Place Published, 1975).
37 Bolton, B. A., Kint, S., Bailey, G. F. & Scherer, J. R. Ethanol sorption and partial molar volume in cellulose acetate films. *J. Phys. Chem.* **90**, 1207-1211 (1986).
38 Linossier, I., Gaillard, F., Romand, M. & Feller, J. F. Measuring water diffusion in polymer films on the substrate by internal reflection fourier transform infrared spectroscopy. *J. Appl. Polym. Sci.* **66**, 2465-2473 (1997).
39 Fieldson, G. T. & Barbari, T. A. The use of FTIR-ATR spectroscopy to characterize penetrant diffusion in polymers. *Polymer* **34**, 1146-1153 (1993).
40 Frezza, L., Patrini, M., Liscidini, M. & Comoretto, D. Directional enhancement of spontaneous emission in polymer flexible microcavities. *J. Phys. Chem. C* **115**, 19939 - 19946 (2011).
41 Bernardo, G. & Vesely, D. Equilibrium solubility of alcohols in polystyrene attained by controlled diffusion. *Eur. Polym. J.* **43**, 938-948 (2007).
42 Daubert, T. E., Danner, R. P., Sibul, H. M. & Stebbins, C. *Physical and Thermodynamical Properties of Pure Chemicals.*, (Taylor and Francis,Place Published, 1988).
43 Brandrup, J., Immergut, E. H., Grulke, E. A., Abe, A. & Bloch, D. R. (John Wiley & Sons New York, 2005).

44 Perrin, L., Nguyen, Q. T., Sacco, D. & Lochon, P. Experimental studies and modelling of sorption and diffusion of water and alcohols in cellulose acetate. *Polym. Int.* **42**, 9-16 (1997).

45 Bernardo, G. Diffusivity of alcohols in amorphous polystyrene. *J. Appl. Polym. Sci.* **127**, 1803-1811 (2013).

46 *3M DICHROIC - https://www.3m.com/3M/en_US/company-us/all-3m-products/~/3M-Dichroic-Films-for-Architectural-Laminated-Glass/?N=5002385+3291680356&rt=rud*.

47 *TORAY - http://www.toray.com/*.

48 *Chamaleonlab - http://chameleonlab.nl/*.

49 Kazmierczak, T., Song, H., Hiltner, A. & Baer, E. Polymeric one-dimensional photonic crystals by continuous coextrusion. *Macromol. Rapid Commun.* **28**, 2210-2216 (2007).

50 *FrinGOe - https://fringoe.com/*.

51 Das, A. J., Wahi, A., Kothari, I. & Raskar, R. Ultra-portable, wireless smartphone spectrometer for rapid, non-destructive testing of fruit ripeness. *Scientific Reports* **6**, 32504 (2016).